# Towards a Novel Edge AI System for Particle Size Detection in Mineral Processing Plants

Flávio Wellb Cardoso[1,2], Mateus Coelho Silva[3], Natália F. de C. Meira[3], Ricardo Augusto Rabelo Oliveira[1,3] and Andrea G. Campos Bianchi[1,3]

[1]*Graduate Program in Instrumentation, Control and Automation of Mining Processes, Instituto Tecnológico Vale, Federal University of Ouro Preto, Ouro Preto, Brazil*

[2]*VALE S.A., Nova Lima, Brazil*

[3]*Department of Computer Science, Federal University of Ouro Preto, Ouro Preto, Brazil*

Keywords: Edge AI, Particle Size Detection, Cloudlets, Mask R-CNN.

Abstract: Monitoring and controlling the particle size is essential to reducing the variability and optimizing energy efficiency in mineral process plants. The industry standard utilizes laboratory processes for particle size characterization; the problems that arise here are obtaining representative sample from the bulk and finding a rapid method of particle size assessment. We propose a machine vision concept based on Edge AI architecture and deep convolutional neural algorithms to enable a real-time analysis of particle size, as an alternative to offline laboratory process. The present paper is part of this proposed concept and aims exclusively to validate a deep convolutional neural network algorithm trained from synthetic datasets. The proposed model reached a mean Average Precision (mAP) of 0.96 and processing times of less than 1s. The results demonstrate the feasibility of deep convolutional neural networks for real-time particle size segmentation and establishes the first step towards a novel Edge AI system for particle size measurement in mineral processing plants.

## 1 INTRODUCTION

In mineral processing, analyzing the particle size of products from operating units is fundamental for determining the quality and optimizing energy efficiency. In comminution[1] operations, for example, the main objective is to release the valuable minerals from their waste gangue[2] in the largest possible size to increase energy efficiency and reduce fines (Wills and Finch, 2015). Necessary plant operation and control changes are made based on the particle size analysis results, either by an operator or an automatic controller (e.g., (Coetzee et al., 2009)).

There are several instruments and methods for laboratory particle size analysis. Some examples of these methods are sieving, laser diffraction, microscopy, gravitational sedimentation, and centrifugal sedimentation(Allen, 2013). However, the characterization of particle sizes in the laboratory presents a range of challenges in terms of time-consuming, expensive bulk sampling equipment, and long response times, limiting the particle size analysis in all critical points, especially in existing plants.

New methods, systems, and equipment have been developed as an alternative to laboratory analysis for particle size characterization. These applications aim to allow real-time, non-intrusive, and low-cost analy-

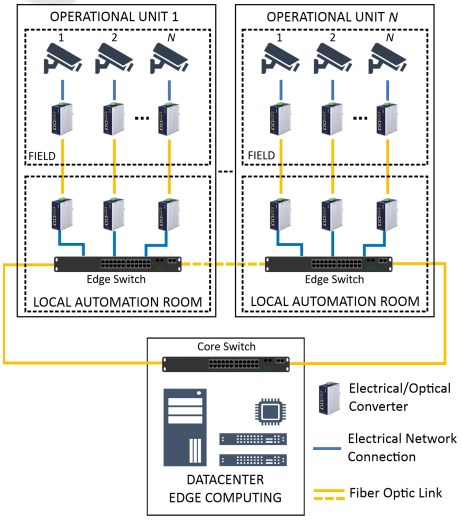


Figure 1: Conceptual Architecture.

[1]comminution: the process of reducing the size of ore particles by crushing or grinding.

[2]gangue: mineral without economic value.



Cardoso, F., Silva, M., Meira, N., Oliveira, R. and Bianchi, A.
Towards a Novel Edge AI System for Particle Size Detection in Mineral Processing Plants.
DOI: 10.5220/0011748000003467
In *Proceedings of the 25th International Conference on Enterprise Information Systems (ICEIS 2023) - Volume 1*, pages 312-323
ISBN: 978-989-758-648-4; ISSN: 2184-4992
Copyright © 2023 by SCITEPRESS – Science and Technology Publications, Lda. Under CC license (CC BY-NC-ND 4.0)

sis (Okada et al., 2020; Al-Thyabat et al., 2007; Thurley and Ng, 2008).

Although significant advances have been made in online particle size measurement by computer vision techniques, challenges to improve accuracy and reduce prediction errors remain in the mineral process due to irregular, noisy, and fuzzy particle ore images caused by adverse environmental conditions, e.g., dust and uneven lighting. Moreover, current market solutions are costly and dependent on specific embedded hardware and close-source software (e.g., (Guyot et al., 2004)).

As an alternative to overcome these previous related challenges, we propose a conceptual architecture design to enable centralized processing of artificial intelligence algorithms, displayed in Figure 1. This concept aims to enable online particle size analysis, by computer vision and deep convolutional neural networks, at all critical points of mineral processing plants. This approach tends to reduce on-site hardware, easily integrate with process control and quality management systems, reduce maintenance costs, increase processing capacity, reduce vulnerability to obsolete hardware, and simplify technology upgrades.

Toward the proposed concept, the present paper aims to validate the deep convolutional neural algorithm as the first step for online particle size analysis based on Edge AI. The advances of this research will include identifying hardware and software requirements to process real-time video images in a centralized cloudlet unit by these artificial intelligence algorithms.

To investigate the feasibility of using a convolutional neural algorithm to segment iron ore particles in complex images, we deployed the Mask R-CNN(He et al., 2017) algorithm, considered a state-of-the-art algorithm for object detection and instance segmentation. The objective is to evaluate the model's accuracy to segment iron ore particles from primary crusher system images. In addition, we propose a synthetic dataset for training and model validation as an alternative to manually labeling data, an exhausting and time-consuming operation needed to attend to a large volume of data required for training.

This paper is organized as follows: Section 2 presents the theoretical references used to complete this work. In Section 3, we overview the most relevant related works recently found in the bibliography. Section 4 presents the experimental methodology applied to validate the convolutional neural network algorithm. In Section 5, we show the results obtained by our approach. Finally, in Section 6 we discuss the results achieved and future improvements.

# 2 THEORETICAL BACKGROUND

The fundamental concept for developing an application with the desired features is Edge AI. This concept relates to several authors' practices in uniting edge computing with artificial intelligence (AI) algorithms to develop solutions for real-world problems (Wang et al., 2020b). Thus, the theoretical references initially cover understanding AI and edge computing and how they can work together toward Edge AI applications.

## 2.1 Edge Computing

In this first subsection of the theoretical references, we provide a definition and evaluation of the concepts within edge computing. We start from the perspective displayed by Khan et al. (Khan et al., 2019). According to these authors, edge computing is a computing landscape concept that brings cloud utilities closer to the edge. Both Khan et at. and Wang et al. (Wang et al., 2020b) recognize three main edge computing perspectives:

- *Cloudlets:* Within this perspective, infrastructures with large computing power provide virtualization of cloud-like services;
- *Fog computing:* This perspective describes the usage of distributed computing to virtualize cloud services;
- *Mobile Edge Computing:* In this case, the services run within isolated edge computing networks or environments.

Although these concepts describe a set of heterogeneous applications, they provide the central premise of edge computing: reducing the latency of a provided service and bringing the processing power closer to the edge. Shi and Dustdar (Shi and Dustdar, 2016) enforce that novel interconnected technologies and perspectives such as the Internet of Things (IoT) have impacted the need for novel edge-based solutions.

## 2.2 Artificial Intelligence (AI)

While edge computing is a relatively new concept, artificial intelligence (AI) has been discussed for decades. McCarthy (McCarthy, 2007) describes AI as the science and technology to create novel intelligent machines. In his concept, intelligence is the ability to learn how to solve a real-world problem through algorithms.

Shinde and Shah (Shinde and Shah, 2018) conceptualize AI as the capability of creating what they de-

scribe as intelligent agents. These agents are capable of maximizing their success opportunities by analyzing environmental variables.

The set of algorithms described by these rules is named machine learning (El Naqa and Murphy, 2015), while the latest set of algorithms within this perspective is named deep learning (LeCun et al., 2015).

## 2.3 Edge AI

There is an increasing interest in uniting the latest deep learning applications within the context of edge computing (Deng et al., 2020). Although AI often uses all possible resources from the device, there is an interest in bringing these services closer to the edge, where computing resources can be limited.

This edge computing and machine learning convergence is named Edge AI (Li et al., 2019). It is also referred to in the literature as edge intelligence (Deng et al., 2020), In-edge AI (Wang et al., 2019), or treated without specific names in other works. This computing perspective requires aspects from edge computing, distributed computing, and AI. Some important constraints in this case are hardware acceleration for AI (Li et al., 2019) and communication (Shi and Dustdar, 2016).

## 2.4 Mask R-CNN

The Mask Regional Convolutional Neural Network (Mask R-CNN) is a meta-algorithm concept proposed by He et al. (2017) (He et al., 2017), a family member of region-based methods for object detection. In general terms, Mask R-CNN uses the framework of Faster R-CNN (Ren et al., 2015), adding a branch for object mask prediction, being executed in parallel with the function of classification and delimitation of this object by the bounding box. Figure 2 shows the basic framework of Mask R-CNN.

The first stage of Mask R-CNN is structured with convolution layers, using a backbone composed of a ResNet101 (He et al., 2015) and a Feature Pyramid Network (FPN) (Lin et al., 2016) that will output a high-resolution feature map. Then, a Region Proposal Network (RPN) is responsible for the Region of Interest (RoI) from the Feature Map, ranking its relevance according to the backbone results.

The result of the RPN is a variable number of RoIs, which in turn will have different dimensions between them, according to the quantity and size of the detected objects. This way, Mask R-CNN resizes the RoIs for the second stage, adjusting them to the dimensions established by the following convolution layers. At this point, the concept proposed by Mask R-CNN brings an essential improvement over the solution usually applied in Faster R-CNN, using the Region of Interest Align (RoIAlign)(Girshick, 2015) method instead of Region of Interest Pooling (RoIPool)(Girshick, 2015) to resize the images. The fundamental difference between the two methods is that RoIAlign can maintain a spatial alignment relationship between the pixels of the input image and the resized output image. This feature of RoIAlign preserves important spatial information, which is responsible for improved mask accuracy from 10% to 50%.

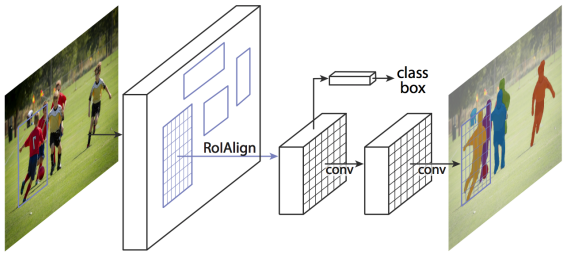


Figure 2: Mask R-CNN Framework(He et al., 2017).

The second stage then starts after the RoIAlign layer, having two distinct branches—the first consists of two Fully Convolutional Network (FCN) (Long et al., 2014) layers being applied to each RoI. As the output of this branch, we will have a binary mask segmenting the object of interest at the pixel level. The second branch performs the object classification and generates the bounding boxes, using a regression method, exactly as performed in Faster R-CNN. The concept of separate branches for classification and segmentation is somewhat of a paradigm break where usually an object is first segmented to be classified. However, He et al. consider this a critical point because, in the loss functions defined, the segmentation process does not compete with the classification.

# 3 RELATED WORKS

In this section, we display some works related to the solution proposed in this paper. Mainly, we study techniques that employ novel computing technologies to perform the same task. We concentrated this section on understanding how other authors use the Mask R-CNN in materials science and mining. Also, we overviewed other deep learning techniques employed in the same areas.

### 3.1 Mask R-CNN Applied to Materials Science and Mining

Huang et al. (Huang et al., 2020) implemented the Mask R-CNN for stockpile aggregate segmentation. The authors manually labeled 164 images (11,795 aggregates) for training and 20 images for validation. The dataset organized by these authors contained aggregates of various geological origins and different sizes, colors, textures, and viewing angles. Detection precision was higher than 87% for all test instances.

Maxwell et al. (Maxwell et al., 2020) combined LiDAR to obtain digital terrain data and the Mask R-CNN algorithm to extract valley fill faces (VFFs), which are a product of mountaintop removal (MTR) coal mining. The precision, recall, and F1-score metrics were above 0.85.

Iyas et al. (Iyas et al., 2020) implemented the Mask R-CNN algorithm to identify rock-forming minerals in images. The authors tested four models, modifying the backbone architecture (ResNet-50 and ResNet-101) and the influence of the lighting on a polarizing microscope. The AP metric was higher for model B (58.0%), which used the lighting on a polarizing microscope and ResNet-101 backbone.

Dong et al. (Dong et al., 2021) proposed a new algorithm for segmenting mineral images of deep sea nodules based on Mask R-CNN. The authors compared it to other deep learning models such as U-Net and Generative Adversarial Network. The experimental results showed that the method based on Mask R-CNN obtained the best results for accuracy, recall, and IoU. U-Net obtained the best result for the precision metric.

Yang et al. (Yang et al., 2021) developed a systematic tool to identify and evaluate images of particles and granular materials that the authors called images of cobble and ballast. First, they used the Mask R-CNN to implement instance segmentation and extract the particle contour. Next, the authors used computational techniques and statistical analysis to evaluate these materials' elongation, angularity, and roughness.

Zhang et al. (Zhang et al., 2019) implemented the Mask R-CNN to segment nanoparticle images from images obtained from the Transmission Electron Microscope. Then the authors fit the contour of the nanoparticles with a circle and measure the size based on that fit.

### 3.2 Deep Learning Applied to Object Segmentation in Materials Science and Mining

Detecting and segmenting particles and agglomerates is a challenge for several areas, especially in materials science, mining and metallurgy. In addition to particle detection, performing the granulometric distribution of these materials is often necessary.

The work by Bukharev et al. (Bukharev et al., 2018) sought to develop a method for segmenting mineral grains in thin-section images of sandstone. The images were obtained using an optical microscope, and the authors implemented the model for a training sample of 9,000 instances. The task consisted of segmenting quasi-convex objects without occlusions. The authors implemented an algorithm based on a cascade of two fully-convolution neural networks (FCNN). The authors used 10-fold validation to test the model's quality. The AP metric was above 76%.

Bamford et al. (Bamford et al., 2021) evaluated the size of rock fragments from blast operations in mines using deep learning strategies. The dataset consisted of labeled images of dynamited rock fragments, 61,853 for training and 1263 for validation. The authors implemented a base architecture of ResNet50. When evaluated using the test suite, the percent error for coarse feature size prediction ranges within ±25%.

Wang et al. (Wang et al., 2020a) used transfer learning and implemented the Mask R-CNN algorithm to monitor open pit mines. The images came from satellite shots. The authors used the ResNet101 network as a backbone.

Frei and Kruis (Frei and Kruis, 2021) introduced the new FibreR-CNN architecture that combines two established R-CNN architectures (Mask and Keypoint R-CNN) to automate the task of analyzing fiber-shaped materials. FibeR-CNN surpassed Mask R-CNN's AP metric by 11 percentage points.

### 3.3 Section Remarks

These works describe applications similar to the proposal of this article, emphasizing that implementations based on deep learning are intensely used as an alternative to conventional methods of computer vision in materials science, mining, and metallurgy. However, they differ in application focus or technique compared to our work. In addition, the industrial environment consists of a complex scenario, and the images present variability, such as occlusion, complex background, rotation, lighting changes, image resolution, and noise (de C Meira et al., 2022).

Validating models and applications as proof of concept in these case studies is still challenging. Our work, therefore, contributes to the advancement of applications in this area.

## 4 EXPERIMENTAL METHODOLOGY

This section presents the experimental methodology suggested for validating the convolutional neural algorithm. For this, we present the dataset development method, the model training strategy, and the applied evaluation metrics. A schematic diagram of the methodology is presented in Figure 3.

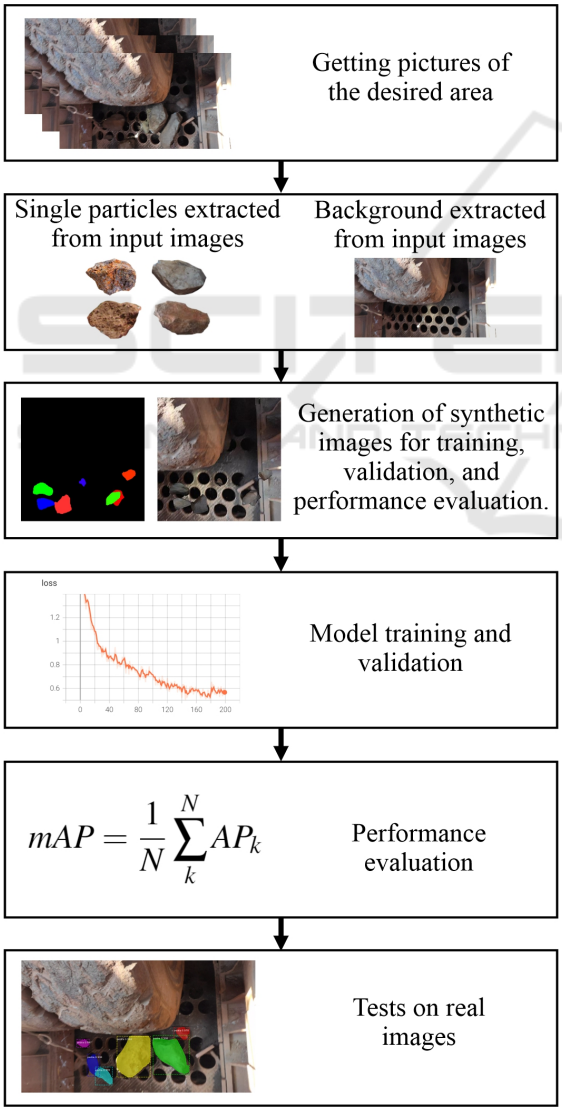


Figure 3: Experimental Methodology Flowchart.

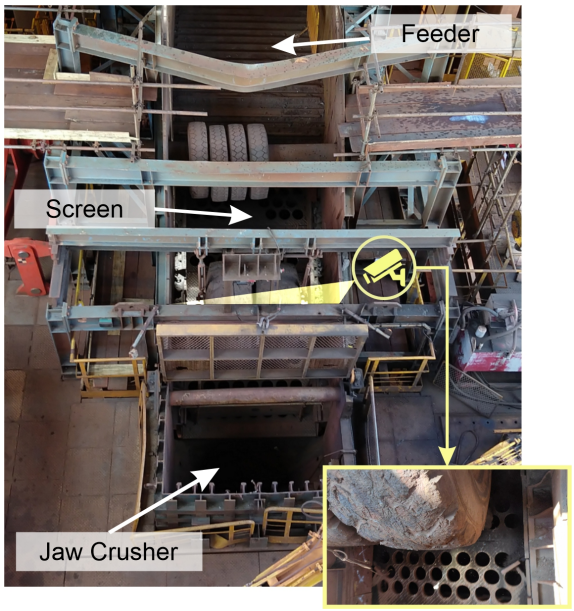


Figure 4: Primary Crusher System.

The study was developed from digital images obtained from a Primary Crushing System showed in Figure 4. The images originate from the primary jaw crusher feed screen, whose ore fragments are in the granulometric range between 200mm and 1000mm. Figure 5 displays a flowchart that represents this process.

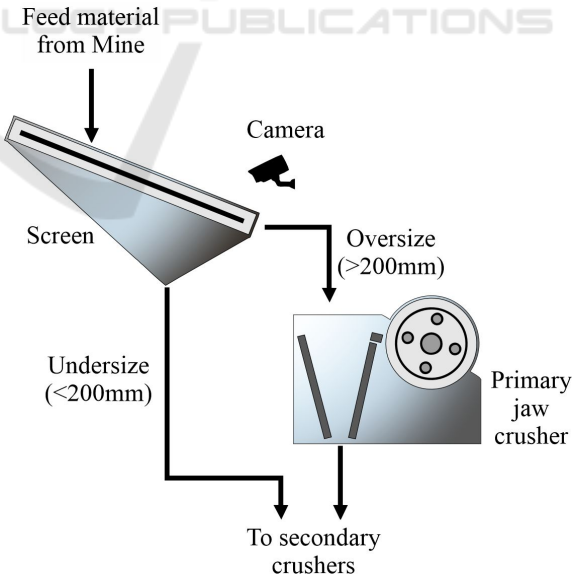


Figure 5: Primary Crusher System.

## 4.1 Dataset

Particular attention was paid to dataset development. As mentioned before, the large volume of data required for training a neural network usually has been the cause of considerable difficulties in obtaining models with high accuracy in the face of manually labeling data.

The synthetic dataset for training the network was developed from real images of the application, obtained from videos recorded at the place of interest and an algorithm[3]. We propose this approach as an alternative to manually labeling data. The algorithm randomly selected the objects from a defined set of foregrounds (iron ore particles) and overlaid them at random positions in the background. During the overlay, rotation, scale, and brightness transformations are applied to the objects.

Using this approach, from a set of 100 objects (fragments) and two backgrounds, the algorithm generated 7,000 images for training and 3,000 for validation (Table 1). Figure 6 presents an example of the synthetic image and its respective mask generated by the algorithm.

Table 1: Dataset composition.

| | Number of images | Annotated regions |
|---|---|---|
| Training | 7,000 | 31,406 |
| Validation | 3,000 | 13,379 |

Figure 6: Example of synthetic image and mask generated.

After composing the image, the algorithm generates the mask of the instantiated objects of each image and the labelings in MS COCO[4] dataset format. This technique makes it possible to generate a considerable amount of synthetic images to be applied to the network training and validation stages.

[3]The algorithm mentioned is an adaptation from open-source code available at https://github.com/akTwelve/cocosynth

[4]Microsoft Common Objects in Context (MS COCO) is a large-scale image dataset

## 4.2 Hyperparameters

The selection of hyperparameters holds a crucial significance in determining the efficacy of the model. The optimization of these values requires a comprehensive grasp of both the input data and the underlying model architecture, as well as a clear comprehension of the desired outcome. The Mask R-CNN [5] was implemented from the original repository available on GitHub, and allow the customization of 48 hyperparameters. The Table2 summarizes the values applied.

Table 2: Hyperparameter values adjusted in Mask R-CNN.

| Variable name in Matterport Implementation | Train 1 and Tain 2 | Train 3 and Train 4 |
|---|---|---|
| LEARNING_RATE | 0.001 | 0.001 |
| BATCH_SIZE | 1 | 1 |
| STEPS_PER_EPOCH | 100 | 100 |
| VALIDATION_STEPS | 10 | 10 |
| NUM_CLASSES | 2 | 2 |
| IMAGE_MIN_DIM | 320 | 320 |
| IMAGE_MAX_DIM | 320 | 320 |
| BACKBONE | resnet50 | resnet101 |
| TRAIN_ROIS_PER_IMAGE | 16 | 16 |
| MAX_GT_INSTANCES | 10 | 10 |

The main adjustments were:

- LEARNING_RATE: The learning rate was kept at its default value of 0.001. This value was deemed suitable as it did not result in instability during training, as demonstrated by the loss curves.
- BATCH_SIZE: refers to the number of samples utilized in a single training step. It was set to 1 to accommodate the GPU's memory constraints. A small batch size typically requires less computational resources to complete an epoch but requires a high number of epochs to converge.
- STEPS_PER_EPOCH: The number of steps per epoch is typically determined by the size of the dataset in relation to the batch size. In this case, the dataset comprises 10,000 images and the batch size is set to 1, resulting in a maximum of 10,000 steps per epoch. However, this is not a practical option as the loss value is only measured at the end of each epoch, which makes it difficult to track the progress of the model's training. To overcome this challenge and effectively monitor the loss, the number of steps per epoch was reduced to 100. This change required an increase in the number of epochs to ensure that the model had sufficient training time to converge and reach stability. With this adjustment, the model's training progress could be monitored more effectively, enabling fine-tuning for optimal performance.

[5]https://github.com/matterport/Mask_RCNN

- IMAGE_MIN_DIM and IMAGE_MAX_DIM: responsible for controlling the resolution of the input image. The default value is 1024x1024. It was adjusted to 320x320 according to the dataset created in MS COCO format.
- BACKBONE: By default, Mask R-CNN uses ResNet101 as its backbone. For comparison purposes, training was done using ResNet101 and ResNet50. Since ResNet101 is deeper, it does have higher memory consumption, longer processing time as well as longer trainning time, however it reaches higher accuracy. On the other hand, ResNet50 has lower memory consumption, shorter processing time and shorter trainning time, hence its accuracy is not as higher as ResNet101.
- TRAIN_ROIS_PER_IMAGE: corresponds to the number of regions of interest generated per image. The default value is 32. It was reduced to 16 as the dataset used in this study only contains a maximum of 16 fragments per image. This adjustment was made with the aim of decreasing training time.
- MAX_GT_INSTANCES: corresponds to the maximum number of instances that can be detected in one image and was set to 10. If the number of instances in the images are limited, this can be set to maximum number of instances that can occur in the image to reduce false positives and training time.

### 4.3 Training the Deep Learning Model

Two training sessions were performed for each backbone configuration (ResNet101 and ResNet50). The initial training was done in 100 epochs (with 100 steps per epoch) using the transfer of learning weights available in MS COCO. In this step, only the head layers were trained as a transfer learning strategy, keeping the weights of the convolutional layers frozen.

After the initial training, a refinement was performed, training the model for another 100 epochs. The fine-tuning step performed the training of the entire network, initializing with the weights obtained from the initial training. Thus, the training of each model was done in two steps, totaling 200 epochs, with 100 steps per epoch. The hardware used was an Intel Core i7-11800H@2.30GHz computer with 64GB RAM.

### 4.4 Evaluation Metrics

In order to generate a graphical representation of the loss values, we used Tensorboard, a Tensorflow toolkit that allows monitoring and visualization of metrics such as loss accuracy. The Mask R-CNN uses three different types of losses as defined in (1). The total loss ($L$) is calculated as the sum of the classification loss ($L_{cls}$), bounding box loss ($L_{box}$), and mask loss ($L_{mask}$) for each object instance in the input image.

$$L = L_{cls} + L_{box} + L_{mask} \tag{1}$$

Where:

$$L_{cls} = L_{cls(RPN)} + L_{cls(mask)}$$
$$L_{box} = L_{box(RPN)} + L_{box(mask)}$$
$$L_{mask} = L_{mask}$$

The mean Average Precision ($mAP$) metric was used to calculate the model's accuracy according to (2), where $N$ represents the number of classes. The Average Precision ($AP$) corresponds to the area under the Precision Vs. Recall curve and could be defined as (3). In turn, the Precision $p(k)$ and Recall $r(k)$ values are calculated according (4) and (5), respectively. Precision measures the accuracy of predictions, while Recall measures the ability of a model to find all objects that should have been detected.

$$mAP = \frac{1}{N}\sum_{k}^{N} AP_k \tag{2}$$

$$AP = \sum_{k=1}^{N} p(k)\left[r(k) - r(k+1)\right] \tag{3}$$

$$p(k) = \frac{TP_k}{TP_k + FP_k} \tag{4}$$

$$r(k) = \frac{TP_k}{TP_k + FN_k} \tag{5}$$

The classification of detections is defined according to the Intersection over Union ($IoU$) metric, presented in (6). If the intersection between the algorithm-generated bounding box and the labeled bounding box is greater than 0.5, the detection will be classified as True Positive ($TP$). If it is less than 0.5, the detection will be classified as False Positive ($FP$), and if there is no detection by the algorithm for any labeled bounding box, it will be classified as False Negative ($FN$).

$$IoU = \frac{Area\ of\ Overlap}{Area\ of\ Union} = \frac{A \bigcap B}{A \bigcup B} \tag{6}$$

# 5 RESULTS

The results of the training sessions were categorized as shown in Table 3, where the highlighted values indicate the lowest value for the selected loss. The overall loss of the model using ResNet50 as its backbone is depicted in Figures 7 and 8 for the training and validation phases, respectively. The model using ResNet101 as its backbone is presented in Figures 9 and 10.

Table 3: Loss values obtained in the training sessions performed.

| LOSSES | | ResNet50 | | ResNet101 | |
|---|---|---|---|---|---|
| Acronym | Variable Name | 100th epoch | 200th epoch | 100th epoch | 200th epoch |
| **Training** | | | | | |
| $L$ | loss | 0,710 | 0,551 | 0,814 | **0,541** |
| $L_{box(mask)}$ | mrcnn bbox loss | 0,144 | **0,106** | 0,148 | 0,107 |
| $L_{cls(mask)}$ | mrcnn class loss | 0,086 | 0,063 | 0,085 | **0,056** |
| $L_{mask}$ | mrcnn mask loss | 0,200 | **0,160** | 0,178 | 0,173 |
| $L_{box(RPN)}$ | rpn bbox loss | 0,269 | 0,212 | 0,384 | **0,197** |
| $L_{cls(RPN)}$ | rpn class loss | 0,012 | **0,010** | 0,019 | 0,056 |
| **Validation** | | | | | |
| $L$ | val loss | 0,845 | **0,521** | 0,806 | 0,682 |
| $L_{box(mask)}$ | val mrcnn bbox loss | 0,119 | **0,087** | 0,154 | 0,100 |
| $L_{cls(mask)}$ | val mrcnn class loss | 0,120 | **0,081** | 0,085 | 0,115 |
| $L_{mask}$ | val mrcnn mask loss | 0,246 | **0,118** | 0,216 | 0,198 |
| $L_{box(RPN)}$ | val rpn bbox loss | 0,354 | **0,227** | 0,335 | 0,262 |
| $L_{cls(RPN)}$ | val rpn class loss | **0,007** | 0,008 | 0,016 | 0,008 |

The effectiveness of the model can be evaluated by analyzing the various losses calculated during the training and validation phases, as described below:

- $L_{cls(RPN)}$ (*rpn class loss*): refers to the loss incurred by the Region Proposal Network's incorrect labeling of anchor boxes as having or not having an object. A low value indicates a high level of accuracy in the model's object detection.
- $L_{cls(mask)}$ (*mrcnn class loss*): refers to the loss incurred due to incorrect labeling of objects within the proposed region. A low value indicates that the detected objects are being accurately classified.
- $L_{box(RPN)}$ (*rpn bbox loss*): refers to the precision of the RPN in placing the bounding box. A low value indicates that the bounding box is accurately positioned on the detected object.
- $L_{box(mask)}$ (*mrcnn bbox loss*): refers to the loss assigned to the placement of the bounding box for a class, as determined by the mask branch. A low value implies a high degree of accuracy in the bounding box's positioning.
- $L_{mask}$ (*mrcnn mask loss*): refers how precisely the masks outline the objects at the pixel level. A low value indicates that the mask accurately fits around the object's boundaries.

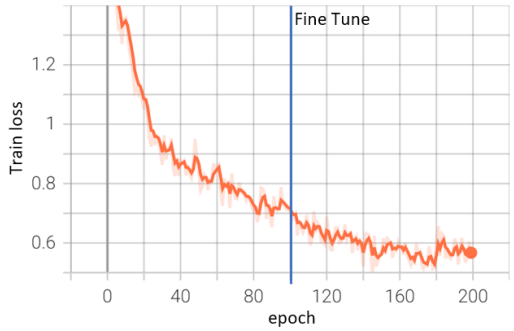


Figure 7: ResNet50 Backbone - overall training loss.

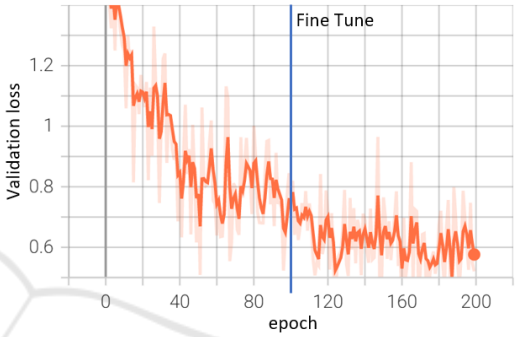


Figure 8: ResNet50 Backbone - overall validation loss.

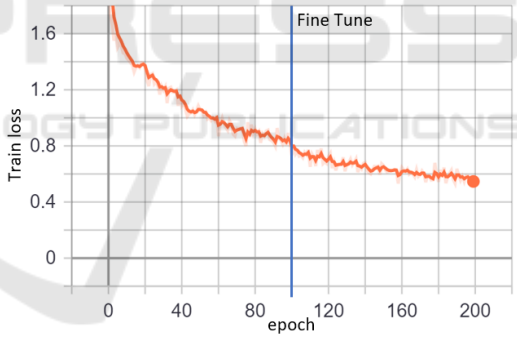


Figure 9: ResNet101 Backbone - overall training loss.

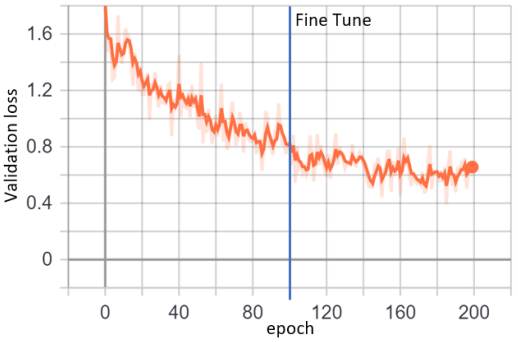


Figure 10: ResNet101 Backbone - overall validation loss.

SCITEPRESS SCIENCE AND TECHNOLOGY PUBLICATIONS

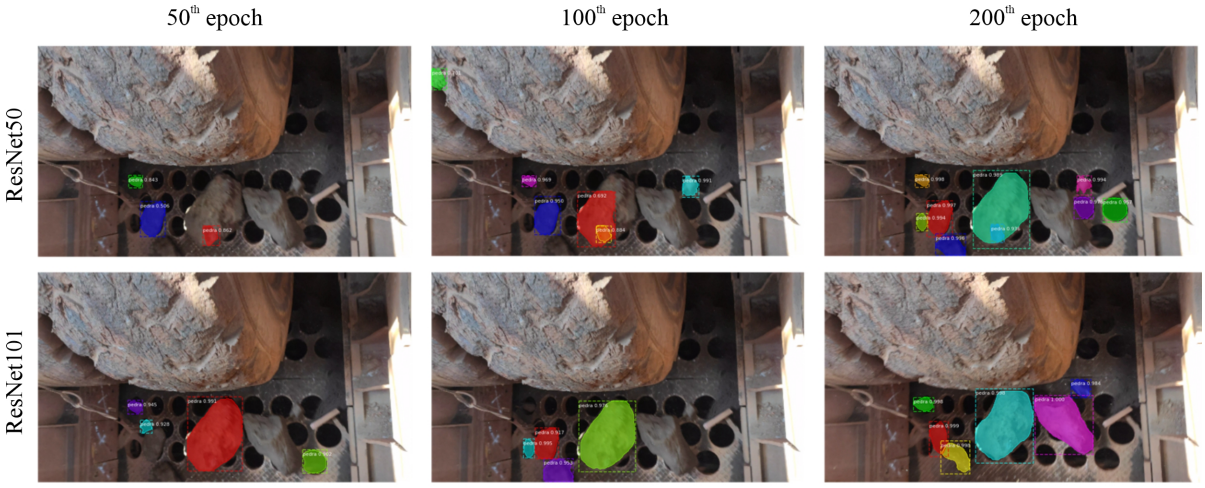


Figure 11: Segmentation performed by Mask R-CNN with ResNet50 and ResNet101.

The loss results presented in Table 3 show that both models are nearly equivalent. Figures from 7 to 10 indicate that the total losses in the training and validation phases converged without any signs of overfitting or underfitting. Additionally, a reduction of approximately 20% in total losses was observed after the 100th epoch, when all layers of the model began training.

The model's performance was evaluated using the *mAP* metric with an *IoU* of 0.5, computed from a dataset of 100 images. The results are presented in Table 4 for the model using ResNet50 as a backbone, and Table 5 for the model using ResNet101 as a backbone.

The mAP scores achieved by both models were similarly close, with the best result achieved by the model using ResNet50 as its backbone in the 200th epoch.

An example of model prediction tests, conducted at different training times and using actual images, is presented in Figure 11. Despite the losses of both models being very similar, the tests on actual images revealed that the model utilizing ResNet101 as a backbone exhibited superior mask adjustment, fewer false positives, and the ability to detect more fragments. However, as shown in Figure 12, the ResNet101 model has an average processing time of around 350*ms* per image, whereas the ResNet50 model takes less than 300*ms* on average, resulting in detection times that are 20% faster.

Souza (Souza, 2020) used several deep learning methods, including SSD, Faster R-CNN, YOLOv3, and U-Net, to detect and segment iron ore fragments. Among these, U-Net achieved the best results, with a total loss of less than 0.5 and an *mAP* metric close to 0.92. However, our work demonstrated that the

Table 4: *mAP* metric obtained for model using ResNet50.

| **Epoch** | *mAP* | **Precision** $p(k)$ | **Recall** $r(k)$ | **TP** | **FP** | **FN** |
|---|---|---|---|---|---|---|
| 50th | 0.951 | 0.82 | 0.95 | 437 | 95 | 23 |
| 100th | 0.947 | 0.90 | 0.93 | 428 | 45 | 30 |
| 150th | 0.960 | 0.91 | 0.95 | 438 | 43 | 21 |
| 200th | 0.962 | 0.92 | 0.96 | 438 | 38 | 20 |

Table 5: *mAP* metric obtained for model using ResNet101.

| **Epoch** | *mAP* | **Precision** $p(k)$ | **Recall** $r(k)$ | **TP** | **FP** | **FN** |
|---|---|---|---|---|---|---|
| 50th | 0.846 | 0.85 | 0.84 | 383 | 68 | 75 |
| 100th | 0.917 | 0.91 | 0.91 | 415 | 39 | 43 |
| 150th | 0.960 | 0.90 | 0.95 | 437 | 48 | 21 |
| 200th | 0.961 | 0.93 | 0.95 | 436 | 33 | 22 |

Mask R-CNN algorithm outperformed the others on the same dataset, achieving an *mAP* of 0.96. Figures 13a and 13b show the prediction results of U-Net and our model, respectively. The superiority of Mask R-CNN in bounding box accuracy and the segmentation of iron ore particles is apparent.

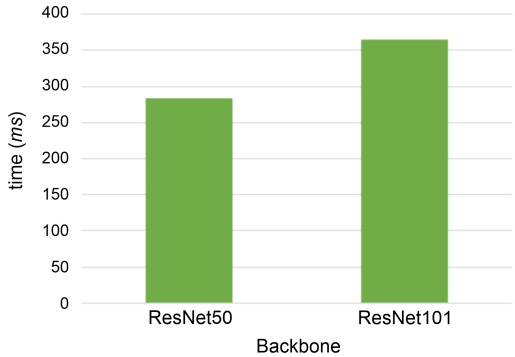


Figure 12: Mean processing time per image.

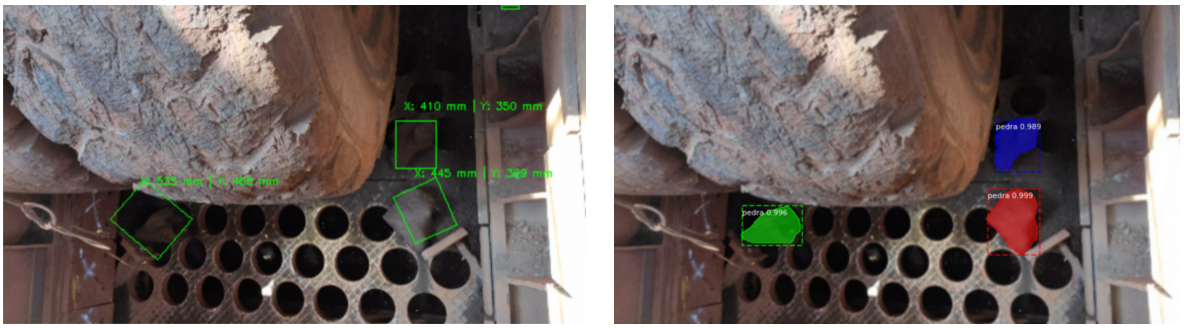


(a) Detection performed by Souza (Souza, 2020) using U-Net (b) Detection performed by Mask R-CNN with ResNet101

Figure 13: Comparative evaluation of results in real images.

# 6 CONCLUSIONS AND FUTURE WORK

This study is a starting point towards a novel Edge AI architecture based on cloudlets to perform particle size detection in mineral processing plants. We proposed this architecture based on the common computing infrastructure present in these plants and validated the algorithm that performed this task.

Edge AI comes from the convergence of edge computing methods and AI algorithms. Edge computing is usually more resource restrained than clouds, while the latest AI algorithms are usually "resource-hungry". Nonetheless, there is an increasing interest in developing solutions combining these concepts to solve real-world problems.

We proposed using a Mask R-CNN algorithm to detect and segment iron ore particles from Primary Crusher System images. The method and results revealed promising aspects for advancing of practical applications for online particle size estimation in mineral processing plants. In a first analysis, we can highlight some relevant points: the synthetic dataset and Mask R-CNN's accuracy.

The proposed dataset's development proved feasible in two aspects: agility in development and capacity dataset augmentation for training. The most significant development of agility refers to traditional image labelling processes, which are too exhaustive in the face of a large amount of data necessary for training convolutional networks.

The use of synthetic datasets in neural network training has several advantages:

- Data Availability: synthetic datasets can be generated easily and in large quantities, even for tasks where collecting real-world data can be challenging or expensive.
- Data Diversity: synthetic datasets can be generated to cover a wide range of scenarios, allowing the model to generalize better to unseen data.
- Data Annotation: synthetic datasets come with ground truth annotations, which makes it easier to train the model and evaluate its performance.
- Data Consistency: the annotations in synthetic datasets are consistent and free of human error, making it easier to evaluate the model's performance objectively.
- Data Augmentation: synthetic datasets can be easily augmented with different variations, such as lighting conditions, background noise, and object deformations, allowing the model to learn from a wider range of scenarios.
- Data Privacy: the use of synthetic datasets can protect sensitive information, such as personal data, that may be present in real-world datasets.

These strategy allowed generating a dataset with 10,000 synthetic images from 102 authentic images in less than 6 hours. The results measured by *mAP* metric as well as the tests on real images, indicates the feasibility of training the model by a synthetic dataset.

The accuracy of applying the Mask R-CNN considering the mAP as a metric was 0.96. We can consider a satisfactory result, considering the network's training in a 100% synthetic dataset. The difference in the results presented by the evaluated backbones (ResNet50 and ResNet101) was not significant in this study.

To further our research, we plan to develop a new synthetic dataset for training, considering the classification of particles in different granulometric ranges. The objective of this new dataset is to enable the Mask R-CNN to perform granulometric classification without additional processing. We hope that further tests will confirm our findings.

Future work will investigate the software performance evaluation to establish the processing and storage hardware requirements for edge computing architecture. Further aspects of this approach, such as integration with the process control system, depend on the evolution of future steps mentioned.

## ACKNOWLEDGMENTS

The authors would like to thank CAPES, Fapemig, CNPq, and the Federal University of Ouro Preto for supporting this work. Also, the authors would like to thank Vale S/A for enabling the creation of a dataset with real images.

This study was financed in part by the Coordenação de Aperfeiçoamento de Pessoal de Nível Superior - Brasil (CAPES) - Finance Code 001, the Conselho Nacional de Desenvolvimento Científico e Tecnológico (CNPQ), the Instituto Tecnológico Vale (ITV) and the Universidade Federal de Ouro Preto (UFOP).

## REFERENCES

Al-Thyabat, S., Miles, N., and Koh, T. (2007). Estimation of the size distribution of particles moving on a conveyor belt. *Minerals Engineering*, 20(1):72–83.

Allen, T. (2013). *Particle size measurement*. Springer.

Bamford, T., Esmaeili, K., and Schoellig, A. P. (2021). A deep learning approach for rock fragmentation analysis. *International Journal of Rock Mechanics and Mining Sciences*, 145:104839.

Bukharev, A., Budennyy, S., Lokhanova, O., Belozerov, B., and Zhukovskaya, E. (2018). The task of instance segmentation of mineral grains in digital images of rock samples (thin sections). In *2018 International Conference on Artificial Intelligence Applications and Innovations (IC-AIAI)*, pages 18–23. IEEE.

Coetzee, L. C., Craig, I. K., and Kerrigan, E. C. (2009). Robust nonlinear model predictive control of a run-of-mine ore milling circuit. *IEEE Transactions on control systems technology*, 18(1):222–229.

de C Meira, N. F., Silva, M. C., Vieira, C. B., Souza, A., and Oliveira, R. A. (2022). Edge deep learning towards the metallurgical industry: Improving the hybrid pelletized sinter (hps) process. In *International Conference on Enterprise Information Systems*, pages 149–167. Springer.

Deng, S., Zhao, H., Fang, W., Yin, J., Dustdar, S., and Zomaya, A. Y. (2020). Edge intelligence: The confluence of edge computing and artificial intelligence. *IEEE Internet of Things Journal*, 7(8):7457–7469.

Dong, L., Wang, H., Song, W., Xia, J., and Liu, T. (2021). Deep sea nodule mineral image segmentation algorithm based on mask r-cnn. In *ACM Turing Award Celebration Conference-China (ACM TURC 2021)*, pages 278–284.

El Naqa, I. and Murphy, M. J. (2015). What is machine learning? In *machine learning in radiation oncology*, pages 3–11. Springer.

Frei, M. and Kruis, F. E. (2021). Fiber-cnn: Expanding mask r-cnn to improve image-based fiber analysis. *Powder Technology*, 377:974–991.

Girshick, R. (2015). Fast r-cnn. cite arxiv:1504.08083Comment: To appear in ICCV 2015.

Guyot, O., Monredon, T., LaRosa, D., and Broussaud, A. (2004). Visiorock, an integrated vision technology for advanced control of comminution circuits. *Minerals Engineering*, 17(11):1227–1235. Communition '04.

He, K., Gkioxari, G., Dollár, P., and Girshick, R. (2017). Mask r-cnn. cite arxiv:1703.06870Comment: open source; appendix on more results.

He, K., Zhang, X., Ren, S., and Sun, J. (2015). Deep residual learning for image recognition. cite arxiv:1512.03385Comment: Tech report.

Huang, H., Luo, J., Tutumluer, E., Hart, J. M., and Stolba, A. J. (2020). Automated segmentation and morphological analyses of stockpile aggregate images using deep convolutional neural networks. *Transportation Research Record*, 2674(10):285–298.

Iyas, M. R., Setiawan, N. I., and Warmada, I. W. (2020). Mask r-cnn for rock-forming minerals identification on petrography, case study at monterado, west kalimantan. In *E3S Web of Conferences*, volume 200, page 06007. EDP Sciences.

Khan, W. Z., Ahmed, E., Hakak, S., Yaqoob, I., and Ahmed, A. (2019). Edge computing: A survey. *Future Generation Computer Systems*, 97:219–235.

LeCun, Y., Bengio, Y., and Hinton, G. (2015). Deep learning. *nature*, 521(7553):436–444.

Li, E., Zeng, L., Zhou, Z., and Chen, X. (2019). Edge ai: On-demand accelerating deep neural network inference via edge computing. *IEEE Transactions on Wireless Communications*, 19(1):447–457.

Lin, T.-Y., Dollár, P., Girshick, R., He, K., Hariharan, B., and Belongie, S. (2016). Feature pyramid networks for object detection. cite arxiv:1612.03144.

Long, J., Shelhamer, E., and Darrell, T. (2014). Fully convolutional networks for semantic segmentation. cite arxiv:1411.4038Comment: to appear in CVPR (2015).

Maxwell, A. E., Pourmohammadi, P., and Poyner, J. D. (2020). Mapping the topographic features of mining-related valley fills using mask r-cnn deep learning and digital elevation data. *Remote Sensing*, 12(3):547.

McCarthy, J. (2007). What is artificial intelligence.

Okada, N., Maekawa, Y., Owada, N., Haga, K., Shibayama, A., and Kawamura, Y. (2020). Automated identification of mineral types and grain size using hyperspectral imaging and deep learning for mineral processing. *Minerals*, 10(9).

Ren, S., He, K., Girshick, R., and Sun, J. (2015). Faster r-cnn: Towards real-time object detection with region

proposal networks. cite arxiv:1506.01497Comment: Extended tech report.

Shi, W. and Dustdar, S. (2016). The promise of edge computing. *Computer*, 49(5):78–81.

Shinde, P. P. and Shah, S. (2018). A review of machine learning and deep learning applications. In *2018 Fourth international conference on computing communication control and automation (ICCUBEA)*, pages 1–6. IEEE.

Souza, L. E. R. (2020). Medição de granulometria de minério de ferro através de imagens em circuito de britagem primária. 2020. Master's thesis, Escola de Minas, Universidade Federal de Ouro Preto, Ouro Preto.

Thurley, M. J. and Ng, K. C. (2008). Identification and sizing of the entirely visible rocks from a 3d surface data segmentation of laboratory rock piles. *Computer Vision and Image Understanding*, 111(2):170–178.

Wang, C., Chang, L., Zhao, L., and Niu, R. (2020a). Automatic identification and dynamic monitoring of open-pit mines based on improved mask r-cnn and transfer learning. *Remote Sensing*, 12(21):3474.

Wang, S., Tuor, T., Salonidis, T., Leung, K. K., Makaya, C., He, T., and Chan, K. (2019). Adaptive federated learning in resource constrained edge computing systems. *IEEE Journal on Selected Areas in Communications*, 37(6):1205–1221.

Wang, X., Han, Y., Leung, V. C., Niyato, D., Yan, X., and Chen, X. (2020b). *Edge AI: Convergence of edge computing and artificial intelligence*. Springer.

Wills, B. A. and Finch, J. (2015). *Wills' mineral processing technology: an introduction to the practical aspects of ore treatment and mineral recovery*, volume 8. Butterworth-Heinemann.

Yang, D., Wang, X., Zhang, H., Yin, Z.-y., Su, D., and Xu, J. (2021). A mask r-cnn based particle identification for quantitative shape evaluation of granular materials. *Powder Technology*, 392:296–305.

Zhang, F., Zhang, Q., Xiao, Z., Wu, J., and Liu, Y. (2019). Spherical nanoparticle parameter measurement method based on mask r-cnn segmentation and edge fitting. In *Proceedings of the 2019 8th international conference on computing and pattern recognition*, pages 205–212.

SCITEPRESS SCIENCE AND TECHNOLOGY PUBLICATIONS